Practical Implications of Using a Solid Electrolyte in Batteries with Sodium Anode: A Combined X-ray Tomography and Model-based Study

*Ronja Haas[a], Constantin Pompe[a,b], Markus Osenberg[c], André Hilger[d], Ingo Manke[d], Boris Mogwitz[a,b], Urmimala Maitra[a,b], Daniel Langsdorf[a,b], Daniel Schröder[a,b]**

[a] R. Haas, Dr. C. Pompe, Dr. B. Mogwitz, Dr. U. Maitra, Dr. D. Langsdorf, Dr. D. Schröder
Institute of Physical Chemistry, Justus Liebig University Giessen, Heinrich-Buff-Ring 17, D-35392 Giessen, Germany
Email: daniel.schroeder@phys.chemie.uni-giessen.de

[b] Dr. C. Pompe, Dr. B. Mogwitz, Dr. U. Maitra, Dr. D. Langsdorf, Dr. D. Schröder
Center for Materials Research (LaMa), Justus Liebig University Giessen, Heinrich-Buff-Ring 16, D-35392 Giessen, Germany

[c] M. Osenberg
Institute of Materials Science and Technology, Technical University Berlin, Hardenbergstraße 36, D-10623 Berlin, Germany

[d] A. Hilger, I. Manke
Helmholtz-Zentrum Berlin für Materialien und Energie GmbH, Hahn-Meitner-Platz 1, D-14109 Berlin, Germany

Keywords: sodium metal anode; solid electrolyte; X-ray tomography; simulation; metal-oxygen battery

Abstract

The commercial use of metal anodes is difficult due to dendrite growth during battery charge, whereas solid electrolytes can be applied as a protective layer to mitigate. Herein X-ray tomography of cycled symmetric sodium cells with Na-β-alumina is used to validate the success of a protective layer. X-ray imaging after cell failure reveals that the solid electrolyte unexpectedly broke apart alongside a crack. The crack might have acted as the nucleation site for sodium dendrite growth, which ended in short-circuiting and cell failure. Operando X-ray radiography is used to reveal that a tilted solid electrolyte is even more likely to break. Simulations complement the experimental study and shed light on the current density distribution at the edges and smallest pinholes. The results obtained emphasize that during fabrication of a battery with protective layer particular care needs to be taken to align the metal electrodes as flat and planar as possible. To achieve the set goal

of fully utilizing a metal anode in future battery technology, much effort has to be made to engineer a proper cell design and accounting for mechanical stress in the solid electrolyte material.

1. Introduction

Rechargeable lithium-ion batteries (LIBs) have been a commercial success as an integral part of all electronic devices due to their up to par energy density and reasonable production costs. Recent years have seen a massive increase in the demand for improved LIBs – especially in view of electromobility and sustainable materials used.[1] Concerns over limited supply and increasing price of lithium led to the demand of alternative battery technologies, e.g. based on sodium. Sodium resources are known to be more available locally, and appeal with high overall abundance and possible lower cost.[1] Sodium ion technology is therefore highly promising and is currently being pursued as one of the sustainable alternatives.[2]

Currently used graphitic/hard carbon anodes provide theoretical capacities of 370 mAh/g for the intercalation of lithium ions.[3] On the contrary, pure metal anodes provide much higher theoretical capacities of 3860 mAh/g and 1160 mAh/g for lithium and sodium, respectively[3], which makes them highly appealing from the practical point of view. However, it is well known that uncontrolled growth of dendrites occurs on metal anodes during battery charging,[4,5] which might lead to short circuits and can trigger thermal runaway in the extreme case[6,7]. The possible next generation of batteries, such as metal-oxygen batteries[8–10] and metal-sulfur batteries[11,12], promise much higher energy densities than current metal ion batteries but also rely on the use of pure metal as anode – exhibiting the same inherent issues and implications of dendrite formation.

Using a solid electrolyte (SE) layer to protect the metal anode might provide a way to mitigate the implications of dendrite growth.[13] Based on the Monroe-Newman model, it is expected that lithium ion conducting SEs with higher shear moduli – at least twice that of lithium metal – can physically suppress the formation of dendrites at the metal surface.[14] Over the past decade researchers worldwide have invested significant efforts in the development of SEs with high ionic conductivity[15,16] comparable to that of liquid electrolytes leading to high expectations for the use of batteries entirely in solid state.[17]

Despite the fact that most of the proposed SEs meet the criterion set by the Monroe-Newman model, solid state batteries and batteries with protected metal anode still suffer from the phenomenon of short-circuiting due to dendrites: Several groups have revealed that lithium dendrites grow into the grain boundaries of SEs like garnet-type LLZO ($Li_7La_3Zr_2O_{12}$[18,19]), while others have pointed out the importance of creating a stable solid-electrolyte-interface (SEI) on the metal anode to avoid dendrite growth.[20] If some grain boundaries reach through the entire SE material, dendrites can even grow through channels that emerge alongside the grains, which might not be possible to suppress at all.[21]

Dendrite formation in batteries with SEs that conduct sodium ions is reported scarcely. Some studies suggest, that the deposition of sodium during electrochemical plating occurs in the micro-cracks and defects in Na-β-alumina type SEs.[22] Failure of Na-β-alumina ceramics was observed as well for sodium sulfur and ZEBRA batteries with molten sodium electrode, but most studies however concentrate on chemical aspects of the stability of the interface between SE and metal.[23–25]

The volume changes during stripping and plating of metal at the anode during cycling and the possible implications for the electrochemistry and for the mechanical stability of the SE are not in the main focus of research on metal anodes yet. For sodium ion batteries however the volume expansion of both the anode and the cathode during the intercalation of sodium ions is considered as one of the main challenges.[26–28]

The herein presented work focuses on monitoring the solid electrolyte in contact with the sodium metal anode during cycling and aims to derive practical guidelines for long-term stable operation. First, cells with sodium metal anode and liquid electrolyte are cycled, investigated in-situ with synchrotron X-ray tomography (similar method as reported elsewhere[29–32]) and with ex-situ surface analytic methods to assess the deleterious effects of dendrite formation as a reference case. Then, Na-β-alumina is introduced to protect the electrodes during cycling. Surprisingly, cell failure occurred similar as observed for the reference case for a multitude of cells. By means of in-situ X-ray tomography and operando X-ray radiography we reveal the underlying cause for cell failure and emphasize the importance to know the mechanical properties of the solid electrolyte materials used. To further shed light on volume changes near the interface of metal anode and solid electrolyte, we present a colligated model-based study. Small holes on the micro-meter scale are identified to strongly affect the current density distribution inside the battery, which

leads to local volume changes and increased mechanical stress for the solid electrolyte during cycling.

Our combined study enables to visualize the processes inside batteries with solid electrolyte at high spatial resolution. Thereby the underlying factors that actually lead to dendrite formation and cell failure are elucidated. This case study shows that even if a protective solid electrolyte layer is applied, dendrite formation occurs so that additional countermeasures during the production and the operation of batteries with solid electrolyte need to be developed. In the end, principal strategies to achieve enhanced cycling stability of next-generation battery types can be extracted from the herein presented work.

2. Results & Discussion

2.1. Cycling behavior without solid electrolyte

We first cycled a symmetric Na/Na cell with polymer separator and liquid electrolyte as a reference case: Three Celgard separators soaked with liquid electrolyte were sandwiched between two Na metal foil electrodes and cycled at a current density of 1.25 mA (1.60 mA cm^{-2}, respectively). **Figure 1**a – being representative for a multitude of cells measured – shows cycling data of such a cell. A typical cell exhibits a potential between 40 - 50 mV during the stripping of sodium ions (occurring at one of the electrodes) and plating of sodium metal (occurring at the respective opposite electrode). In the cell shown in Figure 1a a short circuit occurs after approximately 3,0 mAh of operation as is evidenced by the potential dropping to almost 0 V.

Before the electrochemical measurement and after a few cycles without short circuit, an identically constructed cell with a housing transparent for X-rays (in-situ battery housing made of PTFE; compare methods section) was examined using synchrotron X-ray tomography. Figure 1b shows a sectional view through the center of the cell obtained from the tomography imaging; white colors represent highly attenuating phases for the X-rays or local changes in material density, gray colors represent intermediate attenuation, i.e. ascribed to sodium, the polymer separator or the liquid electrolyte, black colors represent the attenuation of gas phase, which might be incorporated into the sodium metal during preparation. Prior to cycling the separator layers are stacked flat against the sodium electrodes. After a few cycles, we observe significant bending of the stack of separators. It

can be presumed that the continuous and uneven growth/dissolution of Na during stripping/ plating leads to the deformation of the separator layer; i.e. the pristine, planar shape of the Na electrodes cannot be preserved.

Afterwards we analyzed an identically constructed cell with X-ray tomography at regions where dendrites had grown through the separator leading to short circuits (cell cycling shown in **Figure S1**). We observe an accumulation of highly attenuating phases on the top of the separator layers depicted in the sectional view through the center of the cell in Figure 1c. Scanning electron microscopy analysis of the top of the very same separator further sheds light on the nature of the accumulated material: Dense, solid phases have grown, which appear to be the direct result of short-circuiting due to dendrites. The accumulated material mainly contains carbon, sodium and oxygen, which is evidenced by EDX mapping (**Figure S2** in the Supporting Information). **Video file 1** in the Electronic Supporting Information helps to visualize the distribution of the accumulated material across the top of the separators by means of X-ray tomography.

2.2. Cycling with solid electrolyte as protective layer

To improve the cycling stability and avoid short-circuiting for the symmetric cells, the SE Na-β-alumina was applied to act as a physical barrier against dendrite formation. **Figure 2**a shows the results of galvanostatic cycling of such a symmetric Na/Na cell with Na-β-alumina at a current of 0.50 mA (0.64 mA cm^{-2}, respectively). The potential for stripping/plating of sodium ions/sodium for the cell was around 150 - 200 mV, which is significantly higher than for the cell with liquid electrolyte due to the lower ionic conductivity of Na-β-alumina compared to the liquid electrolyte and due to the presumably higher contact resistance between both sides of the SE and the respective sodium electrodes. During the stripping/plating cycles (up to 10 mAh) no signs of dendrite formation can be observed. After subsequent 16 mAh of plating sodium on one of the electrodes the potential drops to almost 0 V, indicating a sudden short circuit between both electrodes.

To examine whether the short circuit was caused by mechanical failure of the SE, the cell was disassembled. Apparently the SE was broken inside the cell so that the top sodium metal electrode was removed carefully and the sole SE was analyzed with highest precaution by means of µCT-X-ray tomography analysis. Figure 2b shows the 3D tomographic image obtained of the SE removed: The Na-β-alumina is shown in beige and sodium phases are

shown in gray. Evidently, a part of the SE is broken off and a large crack of about 6 mm in length has formed. Since additional solid sodium has accumulated inside this crack, the crack might have acted as a nucleation site for the growth of several massive Na dendrites, which could be the reason for short-circuiting and failure of the cell.

We assume that the crack in the SE has formed due to an increase in mechanical stress arising from uneven stripping/plating of sodium ions/sodium metal at the electrodes. In the case of using flexible layers of the Celgard polymer separators this mechanical stress led to bending and deformation of the separator (compare Figure 1b). The flexible polymer separator can easily bend under the increased mechanical stress, whereas the rigid and more brittle Na-β-alumina tends to crack.

To gain further insight on why the SE cracked during extensive cycling, we monitored a symmetric Na/Na cell with Na-β-alumina by synchrotron X-ray radiography during a long-term stripping/plating experiment under with intentionally increased current (compare **Figure 3**a and **video file 2** in the Supporting Information). X-ray radiography enables to view through all layers in the center of the cell during the long-term experiment. Figure 3b depicts the radiographic images in false color obtained at the beginning and at the end of operation. Yellow to orange colors represent low attenuating phase that can be ascribed to sodium (top and bottom, i.e. representing the respective electrodes). Blue to black colors indicate high attenuating phases, which is ascribed to the SE material in the center of the view field. Both radiography images show the same sector of the cell from the same perspective.

A positive current leads to stripping of Na ions from the bottom electrode and to plating of Na metal on the top electrode. Since the entire stack of the electrodes and the SE is kept under constant pressure by stainless steel springs in the operando cell, the associated increase and decrease of electrode volumes demonstrates that the SE moves up and down inside the cell during operation. The deviation of the SEs initial position is extracted from the radiographic images and presented as a shift on the y-axis in Figure 3b.

The capacity put into/extracted from the cell is – according to Faraday's law – in good agreement with the experimentally observed shift in µm (see calculation in the Supporting Information). The difference between the theoretical shift induced by the volume increase/decrease can be explained by the following: At 10 mAh of cycling the SE appears much thicker than initially (0.503 mm vs. 0.565 mm) evidenced by the radiographic images. This is shown in radiography by the blue color values at the edges of the SE. Having blue

instead of black color values in the image implies that the X-rays have not penetrated trough solid material the entire time while passing the operando cell – the SE has simply tilted away from the center point of view instead of directly moving up and down in the 2D plane between the two sodium electrodes. By implication, the uneven stripping/plating of sodium ions/sodium metal at the interface between SE and electrodes led to an unwanted shift of the SE. As a consequence, this tilting of the SE could induce its outer edges to touch other compartments of the cell, e.g. the housing material or the current collector.

An intriguing practical implication is apparent when considering this movement of the SE: Although the cell with two Sodium electrodes and SE was prepared meticulously, the SE is tilted by an angel of approximately 0.3 degrees versus the horizontal axis – a situation that might not even be excluded in high-precision industrial fabrication of future battery types with SE. It comes to mind that if a cell is cycled with tilted SE, the metal electrode on one side of the tilt would be completely stripped away allowing the SE to touch down at one of the current collectors, while some Na metal would still remain on the other end of the tilt. In other words, the SE would be placed on a bearing in between the current collectors. Cycling further in this position would imply increased stress that could ultimately break the SE apart and open pathways for dendrite formation (compare Figure 2). It is to be noted that the manufacturer Ionotec of the Na-β-alumina solid electrolyte used in this work states that a bending strength of around 250 to 350 MPa is needed to break it apart.[33]

2.3. Model-based insight into current density distribution

In another symmetric Na/Na cell with Na-β-alumina we observed, that a hollow region had formed inside the metal electrode where sodium was stripped, evidenced by μCT-X-ray tomography of the entire cell after cycling (compare **Figure S3** for cycling data and **Figure S4** for tomography image). To further understand the processes that led to the formation of such a hollow region, we performed simulations of the current density distribution by means of the software COMSOL and using the AC/DC Module whereas the distribution of the current density is obeying Ohm's law. Simulations were performed for geometry similar as in the operando cells. The results obtained are shown in **Figure 4**.

An ideal symmetric geometry without hollow region inside the metal electrodes was evaluated as reference case (compare Figure 4a). The set current passed between the two electrodes in the simulation was 0.50 mA. The diameter of each electrode was 10 mm so

that the average current density at the outer edges of the geometry is 0.64 mA cm^{-2}. In the middle of the electrode, the current density is distributed homogenously. At the interface of the sodium electrode and the SE, the simulated current density is up to 1.20 mA cm^{-2}, which is only about twice as much as in the middle. Hence, stripping and plating in the ideal symmetric geometry is almost homogeneous and electrochemical reactions will take place predominantly at the edge faces of the two electrodes.

We additionally conducted simulations of geometries with hollow regions inside one electrode, i.e. having 0.15 mm deep cylindrical holes with a diameter of 0.3 mm, 1.0 mm and 5.0 mm inside the bottom sodium electrode, respectively. Figure 4b shows the current density distributions obtained for these geometries: With increasing diameter of the hole the current density in the middle of the electrode is decreasing, whereas the current densities at the edges of the electrode and of the hole are increasing. In all these simulations the current density is highest at the edge faces of the hole. For a hole with a diameter of 5.0 mm, which is approximately the size we observed with the µCT-X-ray tomography (compare **Figure S4**), local values for the current density are up as high as 2.60 mA cm^{-2}. Even with a small pinhole, the maximal local current density is significantly higher than for the simulated reference case. By implication, the electrochemical stripping of sodium ions would be much more enhanced at those spots leading to self-reinforced dissolution of the sodium metal starting from the outer edges of the pinhole – which also makes sense from the viewpoint of surface chemistry since kinks or edges have a lower surface energy and are bound weaker to the material. Consequently, an initial small pinhole will unavoidably grow during battery cycling in every direction of space, which in the end can significantly disturb the interface between sodium electrode and SE.

The formation of a hole in the Na electrode could increase the mechanical stress in the solid electrolyte. Hence, these findings also support the assumption that the crack in the SE was caused by mechanical stress. Furthermore, the non uniform current density distribution because of surface irregularities gives an explanation for the uneven stripping and plating of sodium, which was observed in the cells without solid electrolyte as well.

3. Conclusion

The herein presented study can be used to derive practical guidelines for long-term stable operation of batteries with solid electrolyte. Electrochemical analysis, ex-situ surface analysis

as wells operando and in-situ X-ray tomography and radiography for symmetric cells with two sodium metal electrodes and sodium ion conducting solid electrolyte was applied. The results obtained emphasize that there is a correlation between mechanical deformation of the interface between metal anode and electrolyte, and the formation of dendrites – even if a solid electrolyte is used as protective layer. Projecting the implications of the simulation results to the production of batteries with solid electrolyte and metal anode implies that even smallest pinholes or uneven metal surfaces that could be incorporated during the production and assembly can lead to uneven current density distribution. Thus, even bigger holes can form, destroying the interface between solid electrolyte and metal during battery cycling.

Overall, severe consequences for the practical use of solid electrolytes arise: Mechanically induced stress can cause the formation of a crack deep inside the solid electrolyte, which opens pathways to deposit and agglomerate sodium metal, which in the end leads to self-reinforcing dendrite growth. To manufacture solid state batteries special care needs to be taken to make the metal electrodes as flat and planar as possible, to avoid tilting and to diminish the related increase in mechanical stress on the solid electrolyte, and to avoid that pinholes are incorporated inside the metal electrode during processing. It is also to be noted that since minor tilts and undulations cannot be totally avoided during electrode fabrication and battery assembly, full utilization of the metal anode – the ultimate goal to increase the capacity and energy density of the next generation of batteries – might be hindered in a battery with solid electrolyte.

4. Experimental Section

Cell preparation and electrochemical testing: A Swagelok design cell, also known as 'Giessen cell'[34], consisting of two sodium metal electrodes (Ø = 10 mm, BASF SE) and three polymer separators (Ø = 12 mm, 2340 Celgard) was used. A modified in-situ battery housing made of PTFE was used to enable X-rays to pass through the setup with low attenuation. As electrolyte 20 µL of a solution of 0.5 M sodium triflate (98%, Sigma Aldrich) in diglyme (diethylene glycol dimethyl ether, anhydrous, 99.5%, Sigma Aldrich) was used. The sodium triflate was dried at 175 °C under vacuum for 24 h. In some cells Na-β-alumina (Ø = 12 mm, 0.5 mm thickness, Ionotec) was used as SE. The cells and the electrolyte were prepared in an Argon-filled glove box (GS Systemtechnik) and a Nitrogen-filled glove box (MBraun; used for

X-ray imaging experiments at the beam line only) at water contents below 0.5 ppm and oxygen contents below 1.5 ppm.

Galvanostatic cell cycling was performed at room temperature (25 °C) with battery cycling systems (Maccor 4300 and Ivium Vertex potentiostat/galvanostat). The cycling experiments during the synchrotron X-ray imaging at the beam line was carried out with the Ivium Vertex galvanostat, for all other measurements the Maccor 4300 was used. All current values reported can be converted to current density by using the bottleneck of the cross-sectional areas, the area of the SE or separator, respectively, which is 0.785 cm^2 for the used cell geometry.

Model-based analysis: Simulation of the current density distribution in a geometry with two sodium electrodes (Ø = 10 mm, 0.8 mm thickness) and Na-β-alumina (Ø = 12 mm, 0.3 mm thickness) as SE was performed with COMSOL 5.2 using Multiphysics toolbox with the AC/DC module and the electric current setup. First the simulations were carried out for an ideal symmetrical cell. Then the simulations were repeated with a hole inside the bottom sodium electrode with diameters of 0.3 mm, 1.0 mm and 5.0 mm, respectively. For all simulations a current of 0.5 mA was set between the outer edges of the two sodium electrodes. The conductivity for the different materials was assumed to be $1.1 \cdot 10^7$ S m^{-1} for sodium, 0.1 S m^{-1} for Na-β-alumina and almost insulating with $1 \cdot 10^{-10}$ S m^{-1} for air in the holes in the electrodes.

X-ray analysis: Tomography on the micrometer scale was measured with an in-house designed µCT setup. The pixel sizes are 6.2 µm and 9.7 µm (sample in Figure 2 and sample in Figure S4, respectively). The setup consists of a Hamamatsu L12161-07 cone beam X-ray source with a stable spot size of 5 µm, a HUBER 5-axis translation and rotation stage and a 2,316 x 2,316 pixel Hamamatsu C7942SK-25 flat panel detector with a pixel size of 50 µm equipped with a gadox scintillator screen. Setup control and data acquisition was performed with the software LabView and an in-house evaluation routine. 1,200 projections and additionally 15 dark fields and flat fields have been measured for each sample. For the sample shown in Figure 2 an acceleration voltage of 60 kV and a current of 166 µA was used with an exposure time of 1.9 s and 3 frames per rotation step. The sample shown in Figure S4 was measured with the parameters: 60 kV, 166 µA, 1.9 s and 3 frames. µCT data

normalization and reconstruction was done with the software Octopus 8.9 (Octopus Imaging) using the filtered back projection algorithm. For 3D-visualization VG Studio 3.1 (Volume Graphics) was used.

The radiographies and the tomographies on the submicrometer scale have been measured at BAMline/Bessy II. In the storage ring electron bunches with 1.7 GeV generated synchrotron radiation using a 7 T wavelength shifter, the energy was monochromatized using a double multilayer monochromator resulting in an approximately parallel monochrome (1.7% bandwidth at 20 keV) X-ray beam. The setup of the BAMline endstation consists of a UPM160 translation table with an UPR160a rotation table (Physik Instrumente) and an Optique Peter lens setup with a pco.4000 CCD camera. With a 20 times magnification the setup yields a 1.7 mm x 1.2 mm field of view and a pixel size of 0.438 µm. For the transformation from X-rays to visible light (maximum at 490 nm) a 20 µm thick CdWO4 scintillator was used.

For the high resolution synchrotron tomography as shown in Figure 1 the energy was set to 25 keV. The sample was rotated over 180 degrees while measuring 2200 projections each with an exposure time of 2 seconds. After every 100th projection the measurement was halted and 10 flat fields were measured. For the reconstruction a correlation based algorithm was used to find the best fitting flat field. The normalized data set was then denoised with a 2D total variation filter and reconstructed via filtered back projection (gridrec[35]). Again the software VG Studio 3.1 (Volume Graphics) was used for 3D-visualization.

For the high resolution synchrotron radiography as shown in Figure 3 an energy of 30 keV was used. Over a period of 19 hours 28,698 radiograms and 2,869 flatfields have been measured. Again the flatfields where correlated with the radiograms for normalization optimization. The electrolyte shift has been calculated by tracing the center of mass assuming an isotrope mass distribution. Data post processing and visualization has been done using ImageJ.[36]

It is to be noted that the X-ray radiography measurements impacted the electrochemical processes inside the operando cells slightly. However, the recorded cell potential fluctuates only within a few mV (compare Figure 3a). This is evidenced after approximately 8 mAh of charge within the experiment: The supply of synchrotron X-rays was shut down for a short period of time at the beam line; no X-rays were passing the operando cell and no imaging

data could be recorded during this period and cell potential appeared to be much more stable.

Acknowledgments

The authors gratefully acknowledge financial support by the BMBF (Federal Ministry of Education and Research) within the projects 'BenchBatt' (03XP0047D) and 'MeLuBatt' (03XP0110A). All authors thank the HZB for the allocation of synchrotron radiation beam time and acknowledge the financial support by the HZB during the beam time.

References

[1] P. Adelhelm, P. Hartmann, C. L. Bender, M. Busche, C. Eufinger, J. Janek, *Beilstein J. Nanotechnol.* **2015**, *6*, 1016-1055.

[2] K. Kubota, S. Komaba, *J. Electrochem. Soc.* **2015**, *162*, A2538-A2550.

[3] E. Linden, T. B. Reddy, *Handbook of Batteries*, McGraw-Hill, New York, **2001**.

[4] C. Monroe, J. Newman, *J. Electrochem. Soc.* **2003**, *150*, A1377.

[5] C. Brissot, M. Rosso, J.-N. Chazalviel, P. Baudry, S. Lascaud, *Electrochim. Acta* **1998**, *43*, 1569-1574.

[6] D. P. Finegan, E. Darcy, M. Keyser, B. Tjaden, T. M. M. Heenan, R. Jervis, J. J. Bailey, R. Malik, N. T. Vo, O. V. Magdysyuk, R. Atwood, M. Drakopoulos, M. DiMichiel, A. Rack, G. Hinds, D. J. L. Brett, P. R. Shearing, *Energy Environ. Sci.* **2017**, *10*, 1377-1388.

[7] D. P. Finegan, M. Scheel, J. B. Robinson, B. Tjaden, I. Hunt, T. J. Mason, J. Millichamp, M. Di Michiel, G. J. Offer, G. Hinds, et al., *Nat. Commun.* **2015**, *6*, 6924.

[8] D. Hirshberg, W.-J. Kwak, D. Sharon, M. Afri, A. A. Frimer, H.-G. Jung, D. Aurbach, Y.-K. Sun, *Energy Environ. Sci.* **2016**, 9, 2334-2345.

[9] B. D. McCloskey, J. M. Garcia, A. C. Luntz, *Phys. Chem. Lett.* **2014**, *5*, 1230-1235.

[10] L. Medenbach, C.L. Bender, R. Haas, B. Mogwitz, C. Pompe, P. Adelhelm, D. Schröder, J. Janek, *Energy Technology*. **2017,** 5(12), 2265-74.

[11] C. Waluś, J.-F. Barchasz, J.-F. Colin, E. Martin, J.-C. Elkaïm, E. Leprêtre, *Chem. Commun.* **2013**, *49*.

[12] M. Cuisinier, P.-E. Cabelguen, S. Evers, G. He, M. Kolbeck, A. Garsuch, T. Bolin, M. Balasubramanian, L. F. Nazar, *J. Phys. Chem. Lett.* **2013**, *4*, 3227-3232.

[13] X. Q. Zhang, X. B. Cheng, Q. Zhang, *Adv. Mater. Interfaces* **2018**, *5(2)*, 1701097.

[14] C. Monroe, J. Newman, *J. Electrochem. Soc.* **2005**, *152*, A396.

[15] M. Weiss, D. A. Weber, A. Senyshyn, J. Janek, W. G. Zeier, *ACS Appl. Mater. Interfaces* **2018**, 10 (13), 10935-10944.

[16] S. P. Culver, R. Koerver, T. Krauskopf, W. G. Zeier, *Chem. Mater.* **2018**, 30(13), 4179-4192.

[17] W. G. Zeier, J. Janek, *Nat. Energy* **2016**, *1*, 1-4.

[18] C.-L. Tsai, V. Roddatis, C. Vinod Chandran, Q. Ma, S. Uhlenbruck, M. Bram, P. Heitjans, O. Guillon, *ACS Appl. Mater. Interfaces* **2016**, 8(16), 10617-10626.

[19] S. Yu, R. D. Schmidt, R. Garcia-Mendez, E. Herbert, N. J. Dudney, J. B. Wolfenstine, J. Sakamoto, D. J. Siegel, *Chem. Mater.* **2016**, *28*, 197-206.

[20] B. Wu, S. Wang, J. Lochala, D. Desrochers, B. Liu, W. Zhang, J. Yang, J. Xiao, *Energy Environ. Sci.* **2018**, *11*, 1803-1810.

[21] K. Kerman, A. Luntz, V. Viswanathan, Y.-M. Chiang, Z. Chen, *J. Electrochem. Soc.* **2017**, *164*, A1731-A1744.

[22] M. P. J. Brennan, *Electrochim. Acta* **1980**, *25*, 621-627.

[23] L. C. De Jonghe, L. Feldman, A. Beuchele, *J. Mater. Sci.* **1981**, *16*, 780–786.

[24] L. C. De Jonghe, L. Feldman, A. Buechele, *Solid State Ionics* **1981**, *5*, 267–270.

[25] P. T. Moseley, R. J. Bones, D. A. Teagle, B. A. Bellamy, R. W. M. Hawes, *J. Electrochem. Soc.* **1989**, *136*, 1361–1368.

[26] M. Á. Muñoz-márquez, D. Saurel, J. L. Gómez-cámer, M. Casas-cabanas, E. Castillo-martínez, T. Rojo, *Adv. Energy Mater.* **2017**, *7*, 1700463.

[27] J. Wang, C. Eng, Y. K. Chen-wiegart, J. Wang, *Nat. Commun.* **2015**, *6*, 7496.

[28] S. Kim, D. Seo, X. Ma, G. Ceder, K. Kang, *Adv. Energy Mater.* **2012**, *2*, 710–721.

[29] D. Schröder, C. L. Bender, T. Arlt, M. Osenberg, A. Hilger, S. Risse, M. Ballauff, I. Manke, J. Janek, *J. Phys. D Appl. Phys* **2016**, *49, 404001*.

[30] D. Schröder, C. L. Bender, M. Osenberg, A. Hilger, I. Manke, J. Janek, *Sci. Rep.* **2016**, *6*, 24288.

[31] L. Zielke, F. Sun, H. Markötter, A. Hilger, R. Moroni, R. Zengerle, S. Thiele, J. Banhart, I. Manke, Chem. Electro. Chem. **2016**, 3(7), 1170-1177.

[32] F. Lin, Y. Liu, X. Yu, L. Cheng, A. Singer, O. G. Shpyrko, H. L. Xin, N. Tamura, C. Tian, T.-C. Weng, X.-Q. Yang, Y. S. Meng, D. Nordlund, W. Yang, M. M. Doeff, *Chem. Rev.* **2017**, 117(21), 13123-13186.

[33] Inonotec, Supplier of Na-β-alumina SE, http://www.ionotec.com/conductive-ceramics.html, accessed: November, **2018**

[34] C. L. Bender, P. Hartmann, M. Vračar, P. Adelhelm, J. Janek, *Adv. Energy Mater.* **2014**, 1-10.

[35] B. Dowd, G. Campell, R. Marr, V. Nagarkar, S. Tipnis, L. Axe, D. Siddons, in *Proc. SPIE's Int. Symp. Opt. Sci. Eng. Instrumentation, Vol. 3772*, **1999**, 224-236.

[36] C. T. Rueden, J. Schindelin, M. C. Hiner, B. E. DeZonia, A. E. Walter, E. T. Arena, K. W. Eliceiri, *BMC Bioinformatics* **2017**, *18*, 529.

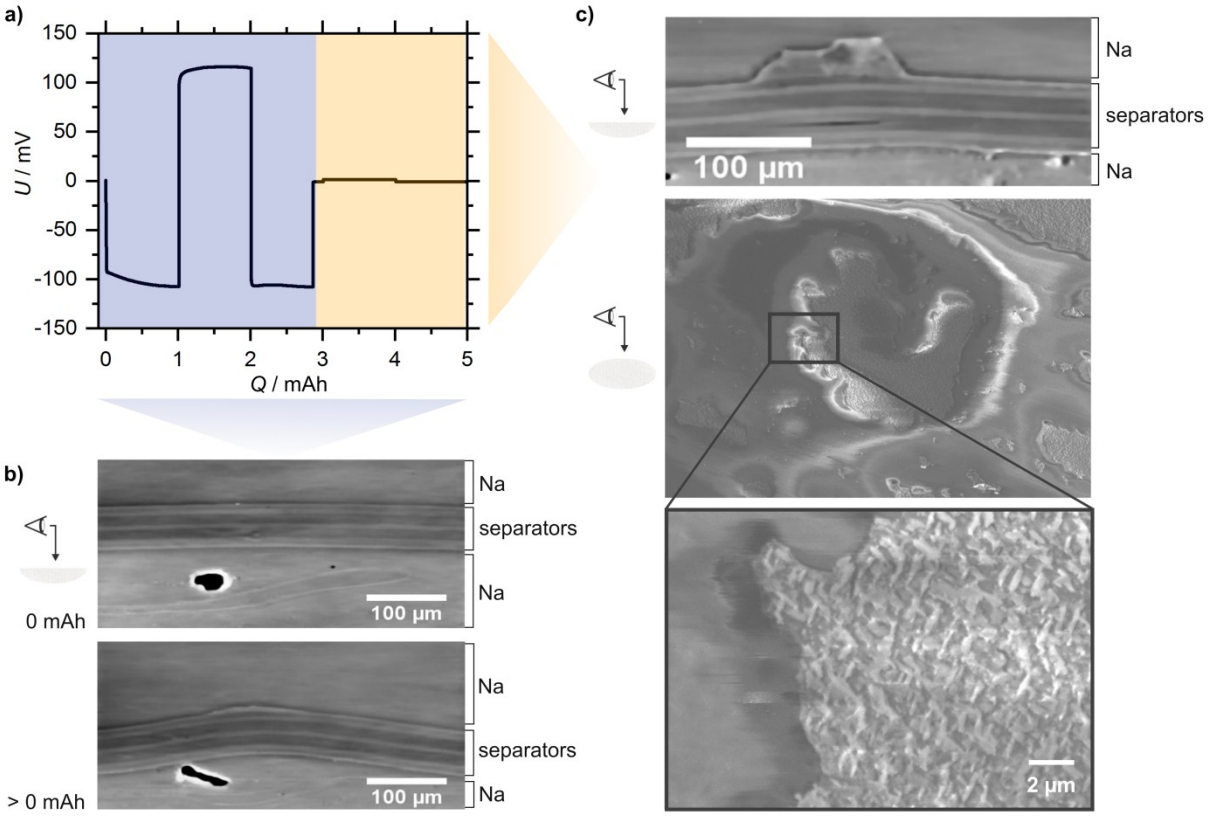

Figure 1.a) Galvanostatic cycling profile of a symmetric Na/Na cell with liquid electrolyte and Celgard separators at 1.25 mA. The blue region indicates the stripping and plating of sodium ions at the two electrodes. The orange region shows the cell potential after a short-circuit. b) Sectional view obtained from in-situ synchrotron X-ray tomography imaging through the center of an identically constructed cell as for Figure 1a showing the stacked layers of Na, polymer separators and Na. Before cycling the Na metal electrodes are planar in shape. After a few cycles the separator layers are bent and deformed. c) Images of the polymer separators after short-circuiting due to dendrite formation. Top panel: Sectional view through the center of the cell; middle and bottom panel: Top view image of the region of the separator where dendrite growth occurred obtained by scanning electron microscopy (electrochemical cycling data for the respective cell shown in Figure S1). Colors in all X-ray tomography images can be interpreted as follows: White colors represent highly attenuating phases for the X-rays, i.e. heavier elements, gray colors represent intermediate attenuation, i.e. ascribed to sodium, polymer separator or liquid electrolyte, black colors represent the attenuation of gas phase, which might be incorporated into the sodium metal during preparation.

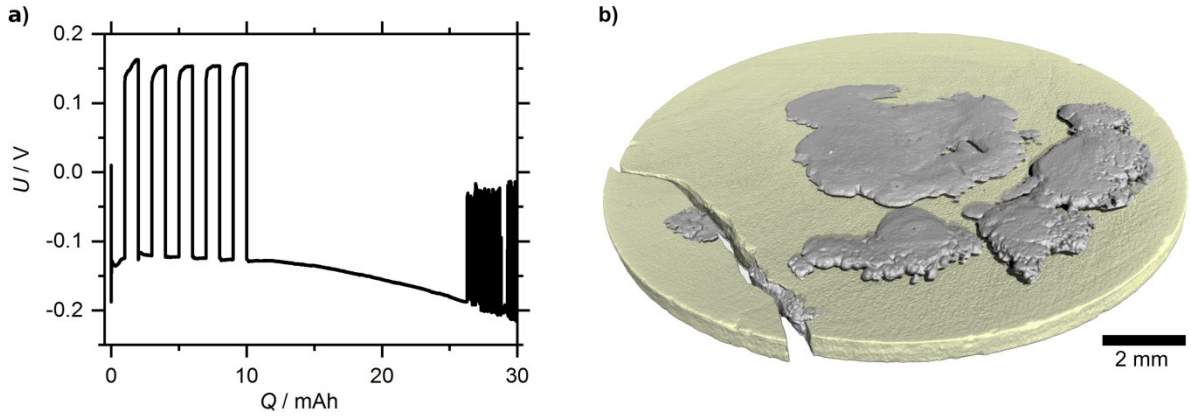

Figure 2. a) Cycling at +/- 0.50 mA of a symmetric Na/Na cell with Na-β-alumina as solid electrolyte. First five discharge/charge cycles where applied and then the cell was discharged until a short circuit appeared and thus cell failure occurred. b) 3D image obtained from ex-situ µCT-X-ray tomography of the solid electrolyte from the same cell after cell failure; presumably the solid electrolyte (beige-colored) broke apart because sodium deposits (gray-colored) have formed within the grain boundaries of the solid electrolyte leading to mechanically induced stress.

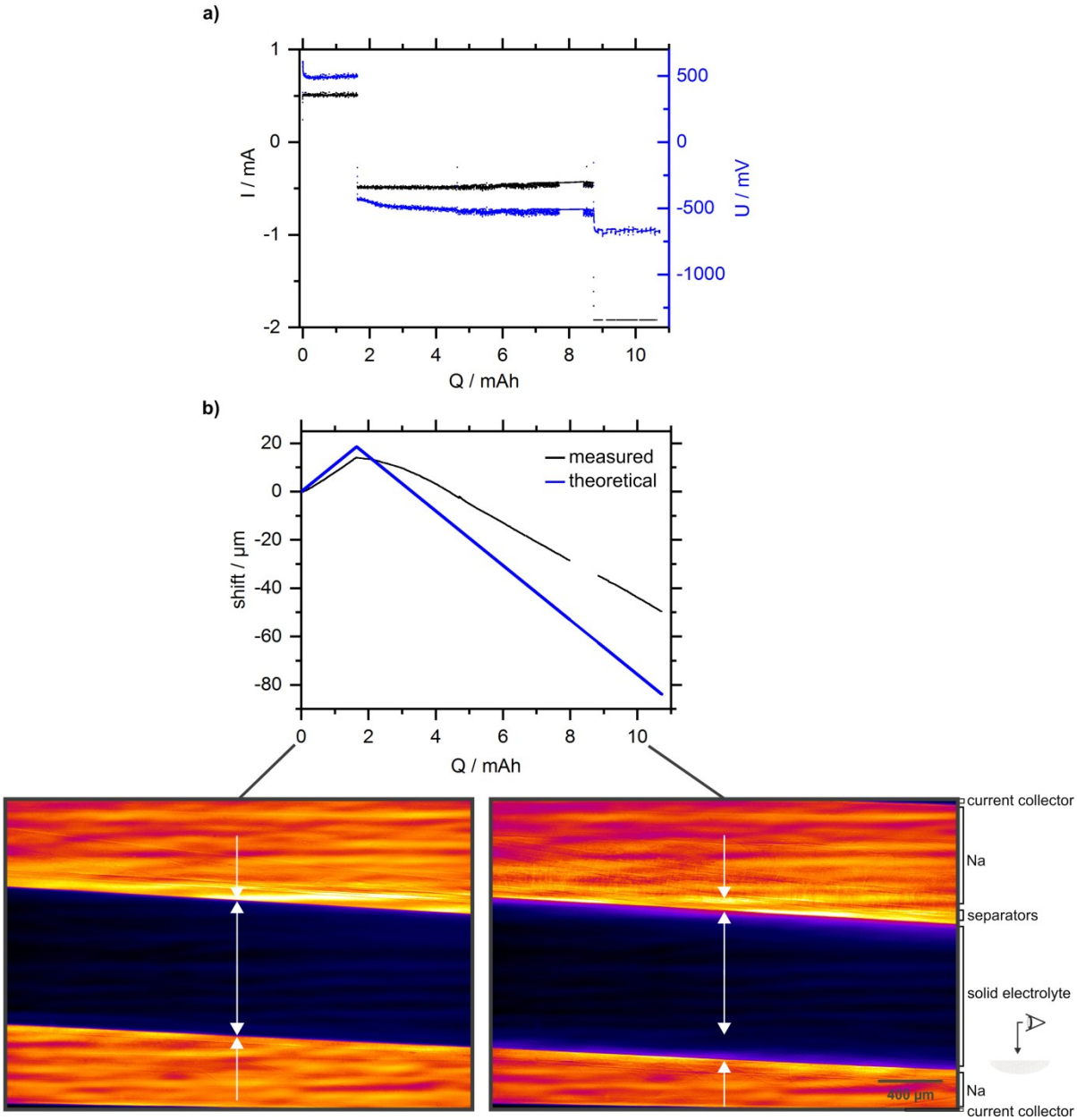

Figure 3. Long-term stripping/plating experiment monitored by synchrotron X-ray radiography of a symmetric Na/Na cell with solid electrolyte as protective layer: a) galvanostatic cycling profile applied and respective response in cell potential; b) Shift of the SEs initial position – using its central point at 0 mAh as zero; extracted from the series of radiographic images taken every 2.37 seconds. Radiographic images indicating the movement of the center of the Na-β-alumina solid electrolyte at the initial stage and at the end of cycling at 10 mAh are shown at the bottom. The view field is thereby 1.7 x 1.2 mm^2 large and yields local information with resolution of 0.438 µm per pixel; yellow to orange colors represent low attenuating phase that can be ascribed e.g. to sodium (top and bottom, i.e. representing the respective electrodes), whereas blue to black colors indicate high attenuating phases, which are ascribed to the SE material. Both radiography images show

the same sector of the cell from the same perspective. The movement of the solid electrolyte is shown as video file 2 in the Electronic Supporting Information available online.

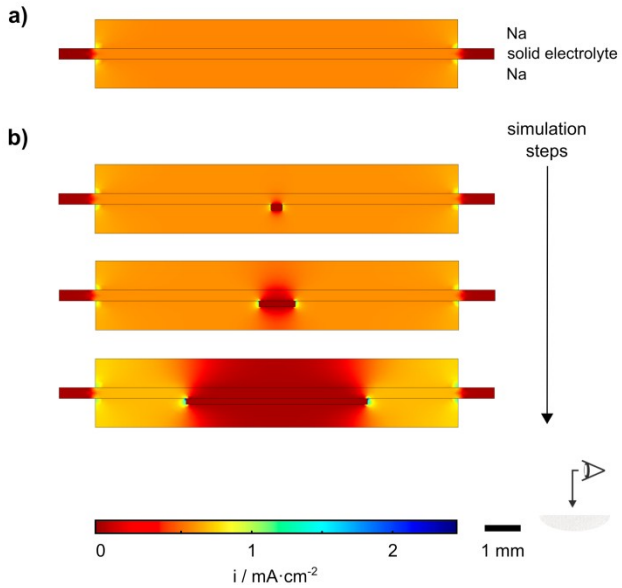

Figure 4. Results of the model-based analysis for a symmetric Na/Na cell with solid electrolyte showing the current density distribution for a fixed current of 0.5 mA between the electrodes. for a) geometry resembling the ideal cell setup with sodium electrode (10 mm diameter), solid electrolyte as separator (12 mm diameter), and another sodium electrode and b) geometry resembling the same setup but with a hole inside the bottom sodium electrode whose diameter is increased step wise for sets of separate simulations from 0.3 mm to 1.0 mm and to 5.0 mm. The color map implies that highest current density are present at the edges of the cell components and near the holes inside the sodium electrode (compare also experimental data for the same geometry in Figure S4).

Additional Electronic Supporting Information

Two files, video 1 (SI_video_1_dendrite_residue.avi) and video 2 (SI_video_2_SE.mp4), are provided online. They help to visualize the accumulated residues on the Celgard separators of a cell after short circuit and the shift of the solid electrolyte during the long-term measurement shown in Figure 3, respectively.

Table of Contents Graphics (TOC)

Ronja Haas, Constantin Pompe, Markus Osenberg, André Hilger, Ingo Manke, Boris Mogwitz, Urmimala Maitra, Daniel Langsdorf, Daniel Schröder*

Practical Implications of Using a Solid Electrolyte in Batteries with Sodium Anode: A Combined X-ray Tomography and Model-based Study

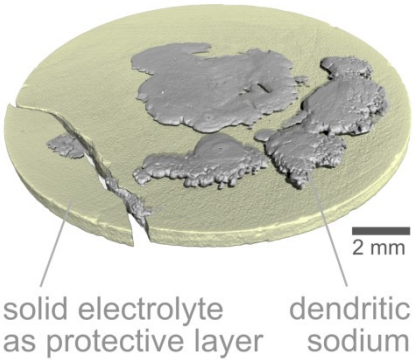

To mitigate dendrite formation a solid electrolyte is used as protective layer on a sodium metal anode. X-ray tomography after cell failure reveals that it unexpectedly broke apart alongside a crack. The results emphasize that fabricating a battery with protective layer can become challenging.

Supporting Information

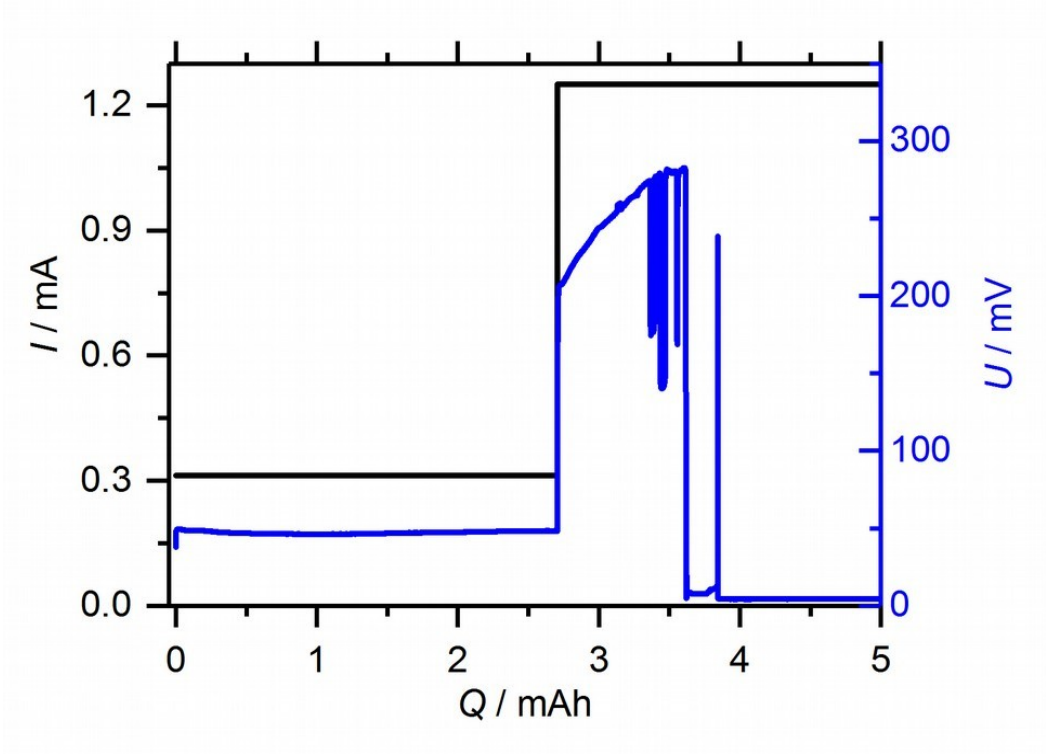

Figure S1: Electrochemical cycling data of the cell shown in Figure 1c.

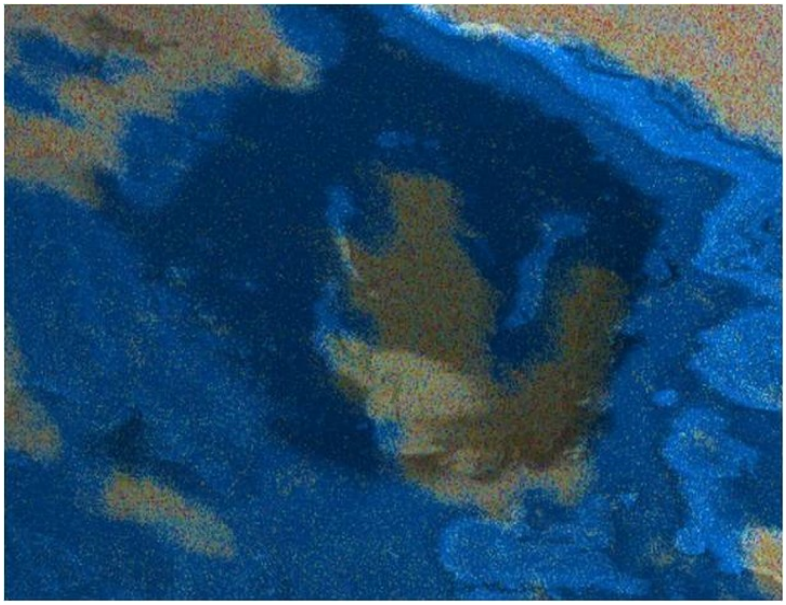

Figure S2: Result of the energy dispersive X-ray spectroscopy mapping of the dense phase that has accumulated on top of the separator after short-circuiting of a symmetric Na/Na cell with liquid electrolyte. The base consists of carbon (blue) whereas the center mainly consists of sodium (red) and a small amount of oxygen (green); scaled as in Figure 1c.

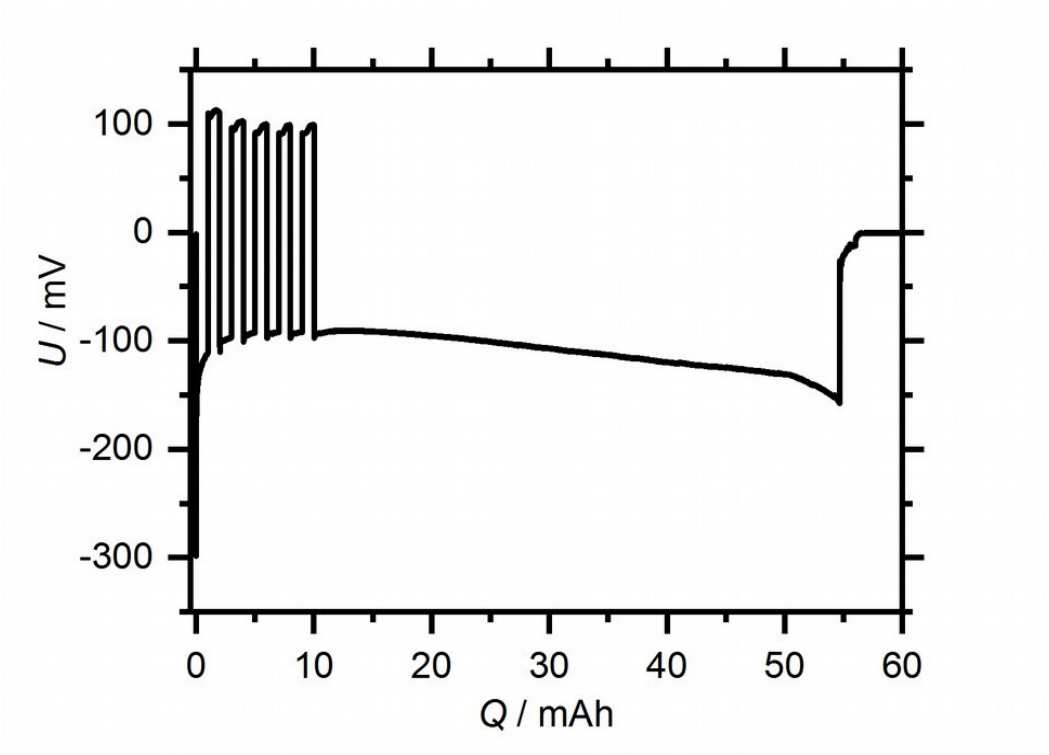

Figure S3: Electrochemical data of the cell shown in Figure S4; galvanostatic cycling for a symmetric Na/Na cell with solid electrolyte at 0.5 mA.

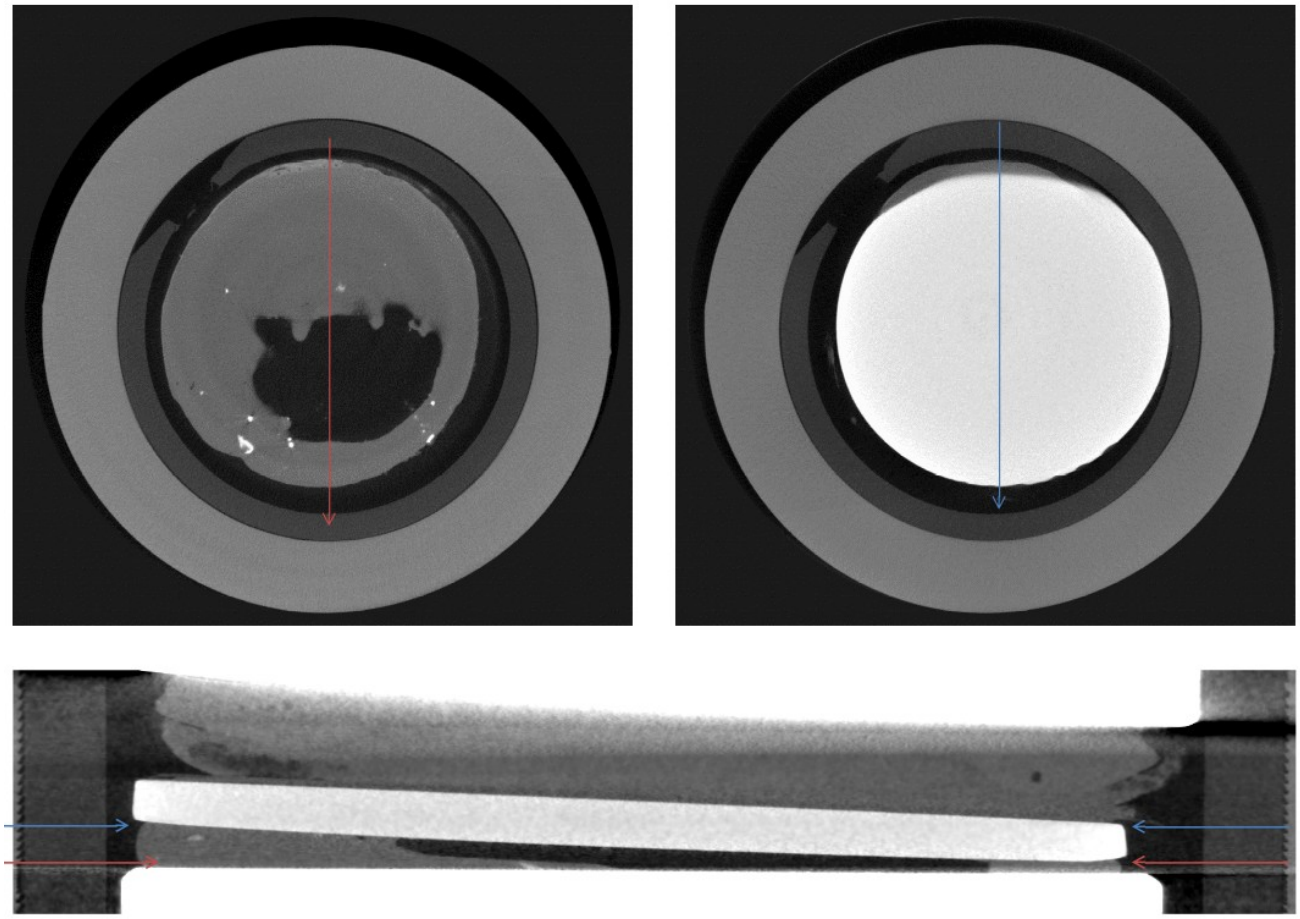

Figure S4: Side view X-ray tomography through the center of the operando cell after discharging (bottom image), whereas the bottom sodium electrode became hollow in its center. White colors represent highly attenuating phases for the X-rays, i.e. the current collector and the solid electrolyte, gray colors represent intermediate attenuation, i.e. ascribed to the sodium metal in the electrodes, black colors represent the attenuation of gas phase, which is e.g. the void space in the operando housing; red and blue arrows indicate the slice direction for the top view images shown in the top part of the figure.

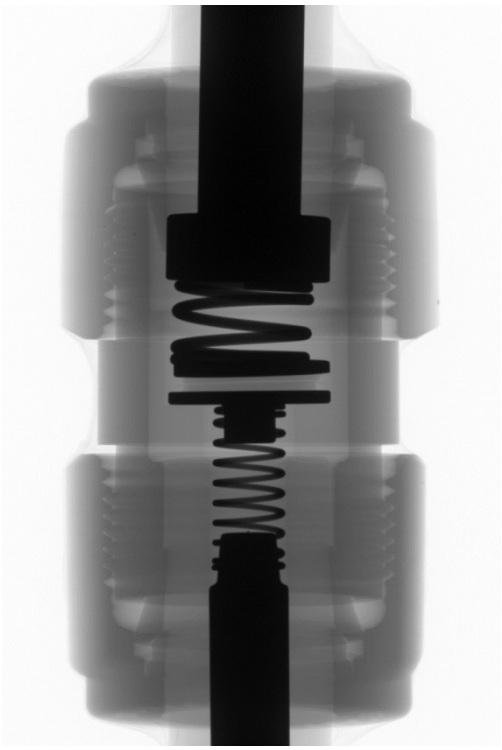

Figure S5: X-ray tomography image showing a sectional view through the center of the applied cell setup with outer current collector, stainless steel spring, stainless steel current collector, battery stack (sodium metal, separator layers, sodium metal), stainless steel current collector, stainless steel spring, outer current collector (from top to bottom); battery housing made of PTFE surrounding the interior.

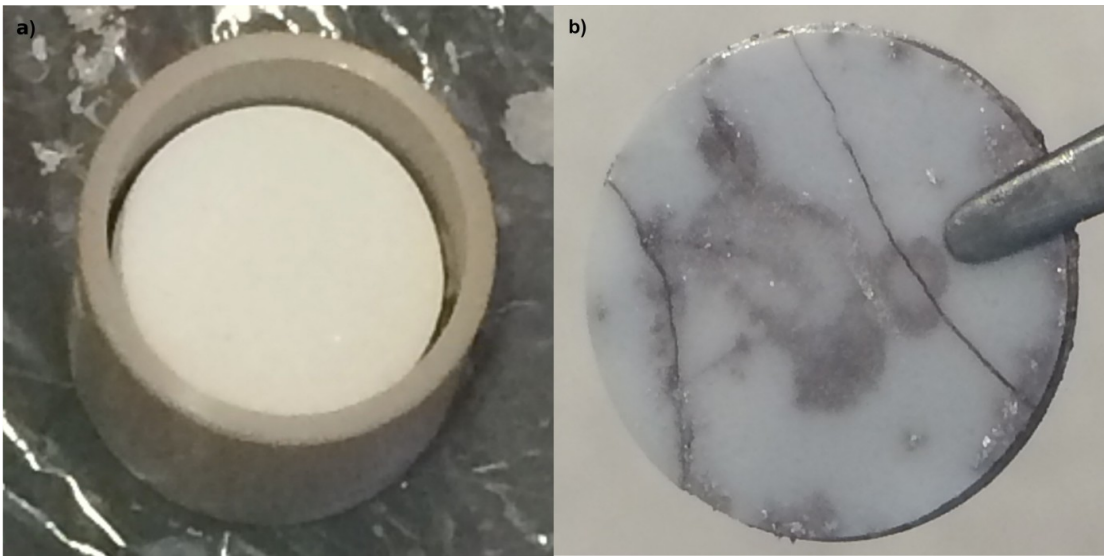

Figure S5: a) *Representative image of an intact solid electrolyte inside the cell interior after pressing it onto the bottom Na electrode in the cell setup.* b) Representative image of a broken Na-β-alumina SE after cycling of a symmetric Na/Na cell at a current of 0.50 mA (0.64 mA cm^{-2}, respectively) for five cycles with 1 mAh each.

Calculation of theoretical shift due to conversion of sodium for Figure 3

The needed capacity Q for the stripping/plating of a certain amount of substance n of ions on an electrode is described with Faraday's law, where z is the charge number and F the Faraday constant.

$$Q = n \cdot z \cdot F$$

The amount of substance of the electrode material n can be calculated with the molar mass M and the density ρ of sodium and the surface area A and the height h of the electrode.

$$n = \rho \cdot \boldsymbol{A} \cdot \boldsymbol{h} \cdot \boldsymbol{M^{-1}}$$

The shift of the SE, Δs, is equal to the height change of the electrode and can therefore be described by the following equation.

$$\Delta s = M \cdot \boldsymbol{Q} \cdot \boldsymbol{\rho^{-1}} \cdot \boldsymbol{A^{-1}} \cdot \boldsymbol{z^{-1}} \cdot \boldsymbol{F^{-1}}$$